

FIRST CONFIRMED DETECTION OF A BIPOLAR MOLECULAR OUTFLOW FROM A YOUNG BROWN DWARF

NGOC PHAN-BAO,¹ BASMAH RIAZ,² CHIN-FEI LEE,¹ YA-WEN TANG,¹ PAUL T.P. HO,^{1,3} EDUARDO L. MARTÍN,^{2,4} JEREMY LIM,¹ NAGAYOSHI OHASHI,¹ HSIEN SHANG¹

Draft version October 27, 2018

ABSTRACT

Studying the earliest stages in the birth of stars is crucial for understanding how they form. Brown dwarfs with masses between that of stars and planets are not massive enough to maintain stable hydrogen-burning fusion reactions during most of their lifetime. Their origins are subject to much debate in recent literature because their masses are far below the typical mass where core collapse is expected to occur. We present the first confirmed evidence that brown dwarfs undergo a phase of molecular outflow that is typical of young stars. Using the Submillimeter Array, we have obtained a map of a bipolar molecular outflow from a young brown dwarf. We estimate an outflow mass of $1.6 \times 10^{-4} M_{\odot}$ and a mass-loss rate of $1.4 \times 10^{-9} M_{\odot}$. These values are over two orders of magnitude smaller than the typical ones for T Tauri stars. From our millimeter continuum data and our own analysis of Spitzer infrared photometry, we estimate that the brown dwarf has a disk with a mass of $8 \times 10^{-3} M_{\odot}$ and an outer disk radius of 80 AU. Our results demonstrate that the bipolar molecular outflow operates down to planetary masses, occurring in brown dwarfs as a scaled-down version of the universal process seen in young stars.

Subject headings: ISM: jets and outflows — ISM: individual (ISO-Oph 102, [GY92] 204) — stars: formation — stars: low mass, brown dwarfs — technique: interferometric

1. INTRODUCTION

Star formation starts with collapse, accretion and launching of material as a bipolar outflow (Lada 1985). It is thought that brown dwarfs could undergo the same stages of formation as stars and that they have a common origin (Luhman et al. 2007). However the typical masses of brown dwarfs, 15–75 M_J , are far below the typical Jeans mass in molecular clouds, and hence it is difficult to make a large number of them by direct gravitational collapse. Several brown dwarf formation mechanisms have been proposed (see Whitworth et al. 2007 and references therein), and more observations are needed to improve our understanding of the role of each of them.

Recent observational evidences for accretion, and optical jets have been found in young brown dwarfs (Martín et al. 2001; Fernández & Comerón 2001; Jayawardhana et al. 2003; Whelan et al. 2007). However there is no firm evidence up to now to demonstrate that the brown dwarf formation involves the bipolar molecular outflow process as seen in young stars. In the case of low-mass stars, the molecular outflow plays a vital role (Bachiller & Gómez-González 1992; Bachiller 1996; Reipurth & Bally 2001; McKee & Ostriker 2007) to testing the low-mass star formation theory (Shu et al. 1991; Masson & Chernin 1993; Raga & Cabrit 1993; Pudritz et al. 2007). Therefore, the detection of molecular outflows provides a key piece of information on the

earliest phase of the brown dwarf formation and allows us to constrain the low-mass star formation theory in the sub-stellar domain.

In this Letter, we present millimeter observations of the young brown dwarf ISO-Oph 102 in the ρ Ophiuchi dark cloud. We detect a bipolar molecular outflow from the brown dwarf, demonstrating that this outflow mechanism as seen in young stars continues to operate down to the masses of brown dwarfs. We show that the outflow mass is much smaller than typical values found in low-mass stars by two to three orders of magnitude. We also combine our radio data with infrared data to estimate disk parameters. The infrared spectrum of ISO-Oph 102 shows strong crystalline silicate features. This demonstrates dust processing in the protoplanetary disk (Apai et al. 2005) of the brown dwarf. The coexistence of the molecular outflow with the crystallization of dust grains could be of importance for models of planet formation.

Sec. 2 presents the millimeter observations and the data reduction, Sec. 3. discusses the physical properties of the bipolar molecular outflow, the disk parameters, and the crystalline silicate features in ISO-Oph 102, Sec. 4 summarizes our results.

2. OBSERVATIONS AND DATA REDUCTION

ISO-Oph 102 (or [GY92] 204), a young M6 dwarf initially identified by Greene & Young (1992), is located in the ρ Ophiuchi dark cloud at a distance of 125 parsecs (de Geus et al. 1989). Its estimated mass is 60 M_J (Natta et al. 2002). This value is below the Hydrogen-burning limit and in good agreement with the dynamically measured mass one of an M6.5 dwarf of 55 M_J at the same age (see Stassun et al. 2005). ISO-Oph 102 is therefore a young bona-fide brown dwarf. The presence of the Lithium absorption in its optical spectrum (Natta et al.

¹Institute of Astronomy and Astrophysics, Academia Sinica, P.O. Box 23-141, Taipei 106, Taiwan, ROC; pbn-goc@asiaa.sinica.edu.tw

²Instituto de Astrofísica de Canarias, C/ Vía Láctea s/n, E-38200 La Laguna (Tenerife), Spain.

³Harvard-Smithsonian Center for Astrophysics, Cambridge, MA

⁴University of Central Florida, Dept. of Physics, PO Box 162385, Orlando, FL 32816-2385

2004) supports its brown dwarf nature (Martín et al. 1994). Strong evidences for the presence of an accretion disk have been reported (Natta et al. 2004). The blue-shifted optical jet component was discovered by Whelan et al. (2005). The optical visibility of ρ Oph 102 suggests that the source corresponds to a class II object (Lada 1985) in the star formation phase, a class with an accreting circumstellar disk and the protostar at this stage is the so-called classical T Tauri star.

We have observed ISO-Oph 102 with the receiver band at 230 GHz of the SMA⁵ (Ho et al. 2004). Both 2 GHz-wide sidebands which are separated by 10 GHz were used. The SMA correlator was configured with high spectral resolution bands of 512 channels per chunk of 104 MHz for ¹²CO, ¹³CO, and C¹⁸O $J = 2 \rightarrow 1$ lines, giving a channel spacing of 0.27 km s⁻¹. A lower resolution of 3.25 MHz per channel was set up for the remainder of each sideband. The quasars 1625–254 and 3C 279 have been observed for gain and passband calibration, respectively. Mars were used for flux calibration. The data were calibrated using the MIR software package and further analysis was carried out with the MIRIAD package adapted for the SMA. The compact configuration was used, resulting a synthesized beam of 3".60 × 2".43 with a position angle of 8.5°. The rms (root mean square) sensitivity was about 3 mJy for the continuum, using both sidebands and ~0.2 Jy beam⁻¹ per channel for the line data. The primary FWHM (full width at half maximum) beam is about 55" at the observed frequencies. The integrated flux density from the dust continuum emission was 7±3 mJy measured at the brown dwarf position.

3. DISCUSSION

An overlay of a near-infrared image and the integrated intensity in the carbon monoxide (CO $J = 2 - 1$) line emission is shown in Figure 1. Two spatially resolved blue- and red-shifted CO components are symmetrically displaced on opposite sides of the brown dwarf position, with the size of each lobe of about 8" corresponding to 1000 AU in length. This is similar to the typical pattern of bipolar molecular outflows as seen in young stars (Lada 1985). The two outflow components with a wide range of velocity (Figure 2) suggests a bow shock structure, an effect of the interaction between the jet propagation and the ambient material, which appears very similar to the bow shock phenomena as seen in young stars (Lee et al. 2000). Such a CO outflow morphology suggests that the jet-driven bow shock model (e.g., Masson & Chernin 1993) may be at work in ρ Oph 102.

Following the standard manner (Cabrit & Bertout 1990; André et al. 1990), we calculate the outflow properties. We use a value of 35 K (Loren et al. 1983) for the excitation temperature, and we derive a lower limit to the outflow mass of $3.2 \times 10^{-5} M_{\odot}$. If we correct for optical depth with a typical value of 5 (Levreault 1988a), we obtain an upper limit to the outflow mass of $1.6 \times 10^{-4} M_{\odot}$. This value is smaller than the ones observed in young stars (Levreault 1988b) by three orders of magnitude.

To estimate the outflow inclination, we combine our SMA data with archival infrared data of the Spitzer

Space Telescope. For the infrared photometry, we use the archival basic calibrated data (PIDs: 58, 177) that were reduced with IRAF⁶ to measure flux densities. Disk modeling is performed as the previous works (see Riaz & Gizis 2008 and references therein). The circumstellar geometry consists of a rotationally flattened infalling envelope, bipolar cavities, and a flared accretion disk in hydrostatic equilibrium. The disk density is proportional to $\varpi^{-\alpha}$, where ϖ is the radial coordinate in the disk midplane, and α is the radial density exponent. The disk scale height increases with radius, $h = h_0(\varpi/R_*)^{\beta}$, where h_0 is the scale height at R_* (the brown dwarf radius) and β is the flaring power. Stellar parameters are obtained from Natta et al. (2004), and an accretion rate of $10^{-9} M_{\odot} \text{ yr}^{-1}$ is used. The NextGen (Hauschildt et al. 1999) atmosphere file for an effective temperature T_{eff} of 2700 K, and $\log g = 3.5$, where g is the surface gravity, is used to fit the atmosphere spectrum of the central sub-stellar source. The disk shows some flaring longward of $\sim 10 \mu\text{m}$, and the best model-fit was obtained using a disk mass of $8 \times 10^{-3} M_{\odot}$, an inclination angle between 63° and 66°, an outer disk radius of 80 AU, and an inner disk radius equal to R_{sub} , where R_{sub} is the dust sublimation radius: $1 R_{\text{sub}} \sim 6.8 R_{\odot}$. There is thus no inner hole in the disk as it would have to be larger than R_{sub} . The outer disk radius and the disk mass are well-constrained by the millimeter observations. A more face-on inclination can be ruled out as it results in larger-than-observed mid- and far-infrared fluxes. Figure 3 presents the best fit from the disk modeling obtained using a disk mass of $8 \times 10^{-3} M_{\odot}$, an inclination angle between 63° and 66°, an outer disk radius of 80 AU, resulting in a projected disk radius of 32-36 AU. This immediately explains the non-detection of the red-shifted optical jet component, estimated to be about 15 AU in length as reported in the previous observation (Whelan et al. 2005). Since the projected disk radius is larger than the jet length, the disk therefore hides the red-shifted jet component from our view.

We use the observed maximum flow velocity of 2.2 km s⁻¹ and apply a correction for the outflow inclination to compute upper limit values for the kinematic and dynamic parameters. We find that the momentum is $P = 1.4 \times 10^{-4} M_{\odot} \text{ km s}^{-1}$, the energy is $E = 3.1 \times 10^{-4} M_{\odot} \text{ km}^2 \text{ s}^{-2}$, the force is $F = 5.9 \times 10^{-8} M_{\odot} \text{ km s}^{-1} \text{ yr}^{-1}$, and the mechanical luminosity is $L = 2.1 \times 10^{-5} L_{\odot}$, where L_{\odot} is the solar luminosity. A correction for the optical depth factor of 5 and a missing flux factor of 3 for SMA (Bourke et al. 2005) will increase these upper limit values by a factor of 15. Using the lower value of the outflow mass and a correction factor of 10 applied for the outflow duration time (Parker et al. 1991), we derive the outflow mass-loss rate of $1.4 \times 10^{-9} M_{\odot} \text{ yr}^{-1}$, which is smaller than a typical value for T Tauri stars (Lada 1985) by two orders of magnitude. One should note that these values are roughly estimated, depending on the correction factor values used in the calculation. One should also note that the outflow mass and the mass loss rate values from ISO-Oph 102 ap-

⁵ The Submillimeter Array is a joint project between the Smithsonian Astrophysical Observatory and the Academia Sinica Institute of Astronomy and Astrophysics and is funded by the Smithsonian Institution and the Academia Sinica.

⁶ IRAF is distributed by the National Optical Astronomy Observatories, which are operated by the Association of Universities for Research in Astronomy, Inc., under cooperative agreement with the National Science Foundation.

pear similar to that from L1014-IRS (Bourke et al. 2005), suggesting that they share the same origin. However as clearly stated in Huard et al. (2006) L1014-IRS could be an embedded protostar or a proto-brown dwarf, corresponding to the earliest stages of star or brown dwarf formation processes, respectively. More observations are needed to confirm the L1014-IRS nature and study the connection between ISO-Oph 102 and L1014-IRS in the whole formation phase.

We also examine the possibility that the emission might be due to bound motions and not outflow emission. This would require an interior mass (Lada 1985) of $2.7M_{\odot}$ for an outflow size of 1000 AU with a velocity of 2.2 km s^{-1} , which is significant larger than the core mass of $< 0.4 M_{\odot}$ within the same radius (Motte et al. 1998; Young et al. 2006). We therefore conclude that the detected emission is from the outflow.

The IRS infrared ($7.5\text{-}14.3 \mu\text{m}$) (Houck et al. 2004) spectra of ISO-Oph 102 whose the basic-calibrated data were downloaded from the Spitzer archive (PID: 3499) and reduced using the SMART software package (Higdon et al. 2004) are also analyzed. It is worthy to note here that the mid-infrared spectrum of ISO-Oph 102 shows crystalline silicate features: enstatite (MgSiO_3) at $9.3 \mu\text{m}$ and very strong forsterite (Mg_2SiO_4) at $11.3 \mu\text{m}$ (see Figure 4). The brown dwarf is indeed an analog of SST-Lup3-1, which is an M5.5 brown dwarf in the Lupus III dark cloud (Merín et al. 2007). The crystalline contribution to the silicate feature (flux at $11.3 \mu\text{m}$ over flux at $9.8 \mu\text{m}$) in ISO-Oph 102 is 1.1, even greater than the value of 0.9 in SST-Lup3-1 (Merín et al. 2007). This provides a direct evidence of grain growth and dust settling, indicating the object is in the transition phase between the class II and III (a class with an optically thin disk) and the brown dwarf is reaching the final mass.

4. SUMMARY

Here, we report the first confirmed detection of the bipolar molecular outflow in young brown dwarfs. We characterize the fundamental properties of the outflow with the first insight on its morphology. The results indicate that the bipolar molecular outflow in brown dwarfs is very similar to outflows as seen in young stars but scaled down by three and two orders of magnitude for the outflow mass and the mass-loss rate, respectively. We demonstrate for the first time that brown dwarfs, even young planetary mass objects (Martín et al. 2001) can launch a bipolar molecular outflow, and hence we confirm that they are likely to have a common origin with the low-mass stars. This suggests that the terminal stellar/brown dwarf mass is not due to different formation mechanisms, but more likely due to the initial mass of the cloud core. We also show that there is evidence for dust crystallization in the disk around the brown dwarf. In brown dwarfs the molecular outflows may be longer lived than in low-mass stars and they coexist with grain growth and crystallization. Outflows from brown dwarfs may play a crucial role in sweeping out gas from the disk and favouring the formation of rocky planets.

NP-B has been aided in this work by a Henri Chrétien International Research Grant administered by the American Astronomical Society. This work is based in part on observations made with the Spitzer Space Telescope, which is operated by the Jet Propulsion Laboratory, California Institute of Technology, under a contract with NASA. This work has made use of the Centre de Données astronomiques de Strasbourg (CDS) database.

REFERENCES

- André, P., Martín-Pintado, J., Despois, D., Montmerle, T. 1990, *A&A*, 236, 180
- Apai, D., Pascucci, I., Bouwman, J., Natta, A., Henning, T., Dullemond, C. P. 2005, *Science*, 310, 834
- Bachiller, R., & Gómez-González, J. 1992, *ARA&A*, 3, 257
- Bachiller, R. 1996, *ARA&A*, 34, 111
- Bourke, T. L., Crapsi, A., Myers, P. C., Evans, Neal J., II, Wilner, D. J., Huard, T. L., Jørgensen, J. K., & Young, C. H. 2005, *ApJ*, 633, L129
- Cabrit, S., & Bertout, C. 1990, 348, 530
- de Geus, E. J., de Zeeuw, P. T., & Lub, J. 1989, *A&A*, 216, 44
- Fernández, M., & Comerón, F. 2001, *A&A*, 380, 264
- Fernández, M., & Comerón, F. 2005, *A&A*, 440, 1119
- Greene, T.P., & Young, E. T. 1992, *ApJ*, 395, 516
- Hauschildt, P. H., Allard, F., Barron, E. 1999, *ApJ*, 512, 377
- Higdon, S. J. U., et al. 2004, *PASP*, 116, 975
- Ho, P. T. P., Moran, J. M., & Lo, K. Y. 2004, *ApJ*, 616, L1
- Houck, J. R., et al. 2004, *ApJS*, 154, 18
- Huard, T. L., et al. 2006, *ApJ*, 640, 391
- Jayawardhana, R., Mohanty, S., & Basri, G. 2003, *ApJ*, 592, 282
- Lada, C. J. 1985, *ARA&A*, 23, 267
- Lee, C.-F., Mundy, L. G., Reipurth, B., Ostriker, E. C., & Stone, J. M. 2000, *ApJ*, 542, 925
- Levreault, R. M. 1988a, *ApJS*, 67, 283
- Levreault, R. M. 1988b, *ApJ*, 330, 897
- Loren, R. B., Sandqvist, A., & Wootten, A. 1983, *A&A*, 270, 620
- Luhman, K. L., Joergens, V., Lada, C., Muzerolle, J., Pascucci, I., & White, R. 2007, in *Protostars and Planets V*, ed. B. Reipurth, D. Jewitt, & K. Keil (Tucson: Univ. Arizona Press), 443
- Martín, E.L., Dougados, C., Magnier, E., Ménard, F., Magazzù, A., Cuillandre, J.-C., Delfosse, X. 2001, *ApJ*, 561, L195
- Martín, E. L., Rebolo, R., & Magazzù, A. 1994, *ApJ*, 436, 262
- Masson, C. R., Chernin, L. M. 1993, *ApJ*, 414, 230
- McKee, C. F., & Ostriker, E. C. 2007, *ARA&A*, 45, 565
- Merín, B., et al. 2007, *ApJ*, 661, 361
- Motte, F., André, P., & Neri, R. 1998, *A&A*, 336, 150
- Natta, A., Testi, L., Comerón, F., Oliva, E., D'Antona, F., Baffa, C., Comoretto, G., Gennari, S. 2002, *A&A*, 393, 597
- Natta, A., Testi, L., Muzerolle, J., Randich, S., Comerón, F., Persi, P. 2004, *A&A*, 424, 603
- Parker, N. D., Padman, R., Scott, P. F. 1991, *MNRAS*, 252, 442
- Pudritz, R. E., Ouyed, R., Fendt, Ch., Brandenburg, A. 2007, in *Protostars and Planets V*, ed. B. Reipurth, D. Jewitt, & K. Keil (Tucson: Univ. Arizona Press), 277
- Raga, A. C., & Cabrit, S. 1993, *A&A*, 278, 267
- Reipurth, B., & Bally, J. 2001, *ARA&A*, 39, 403
- Riaz, B., Gizis, J. E. 2008, *ApJ*, 681, 1584
- Shu, F. H., Ruden, S. P., Lada, C. J., & Lizano, S. 1991, *ApJ*, 370, L31
- Stassun, K. G., Mathieu, R. D., & Valenti, J. A. 2005, *Nature*, 440, 311
- van Boekel, R., Waters, L. B. F. M., Dominik, C., Bouwman, J., de Koter, A., Dullemond, C. P., Paresce, F. 2003, *A&A*, 400, L21
- Whelan, E. T., Ray, T. P., Bacciotti, F., Natta, A., Testi, L., Randich, S. 2005, *Nature*, 435, 652
- Whelan, E. T., Ray, T. P., Randich, S., Bacciotti, F., Jayawardhana, R., Testi, L., Natta, A., Mohanty, S. 2007, *ApJ*, 659, L45
- Whitworth, A., Bate, M. R., Nordlund, Å., Reipurth, B., & Zinnecker, H. 2007, in *Protostars and Planets V*, ed. B. Reipurth, D. Jewitt, & K. Keil (Tucson: Univ. Arizona Press), 459
- Young, K. E., et al. 2006, *ApJ*, 644, 326

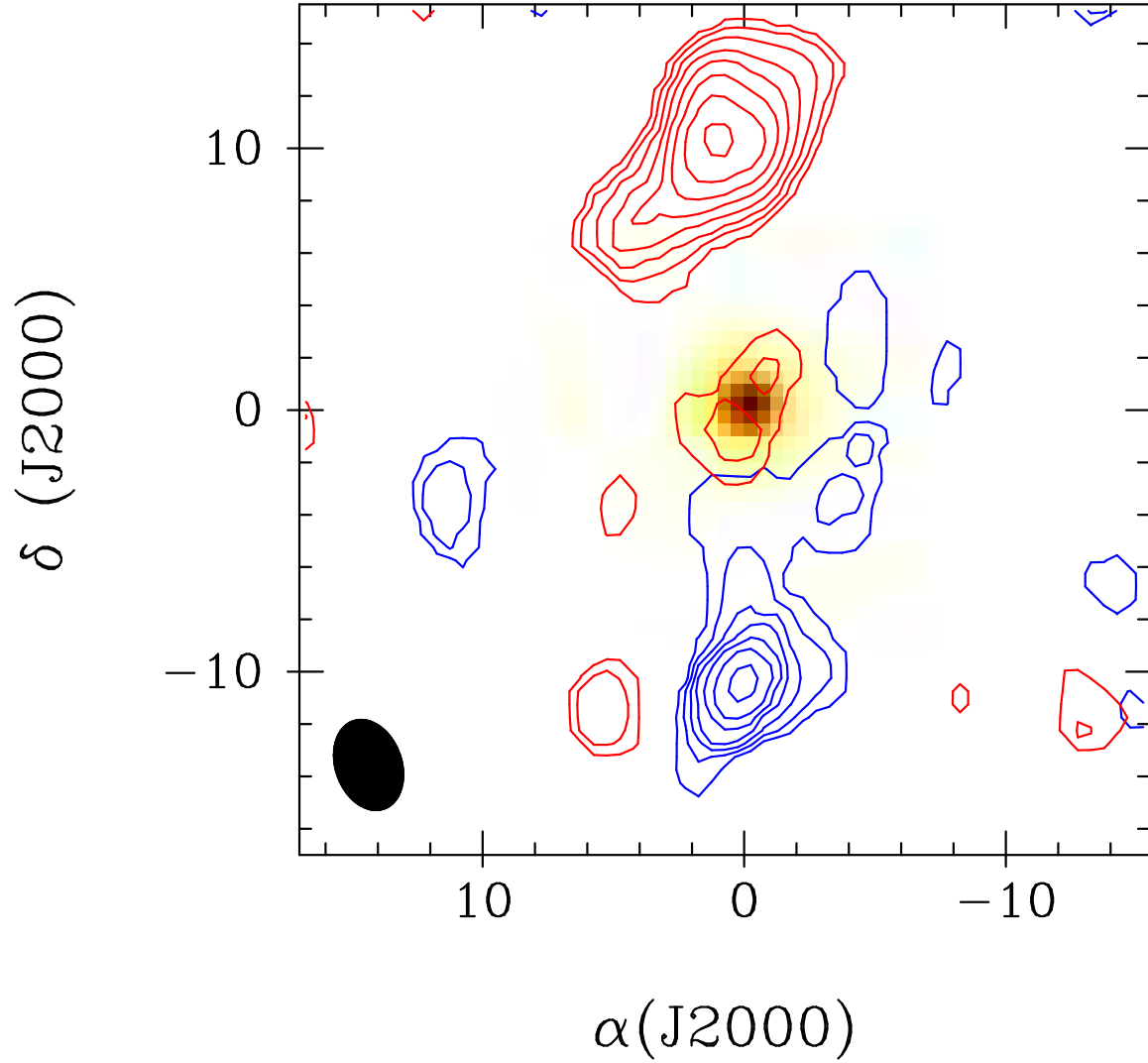


FIG. 1.— An overlay of the J-band ($1.25 \mu\text{m}$) near-infrared Two Micron All Sky Survey (2MASS) image and the integrated intensity in the carbon monoxide ($\text{CO } J = 2 - 1$) line emission from 3.8 to 7.7 km s^{-1} line-of-sight velocities. The blue and red contours represent the blue-shifted (integrated over 3.8 and 5.9 km s^{-1}) and red-shifted (integrated over 5.9 and 7.7 km s^{-1}) emissions, respectively. The contours are $3, 6, 9, \dots$ times the rms of $0.15 \text{ Jy beam}^{-1} \text{ km s}^{-1}$. The brown dwarf is visible in the J-band image. The position angle of the outflow is about 3° . The peaks of the blue- and red-shifted components are symmetric to the center of the brown dwarf with an offset of $10''$. The synthesized beam is shown in the bottom left corner.

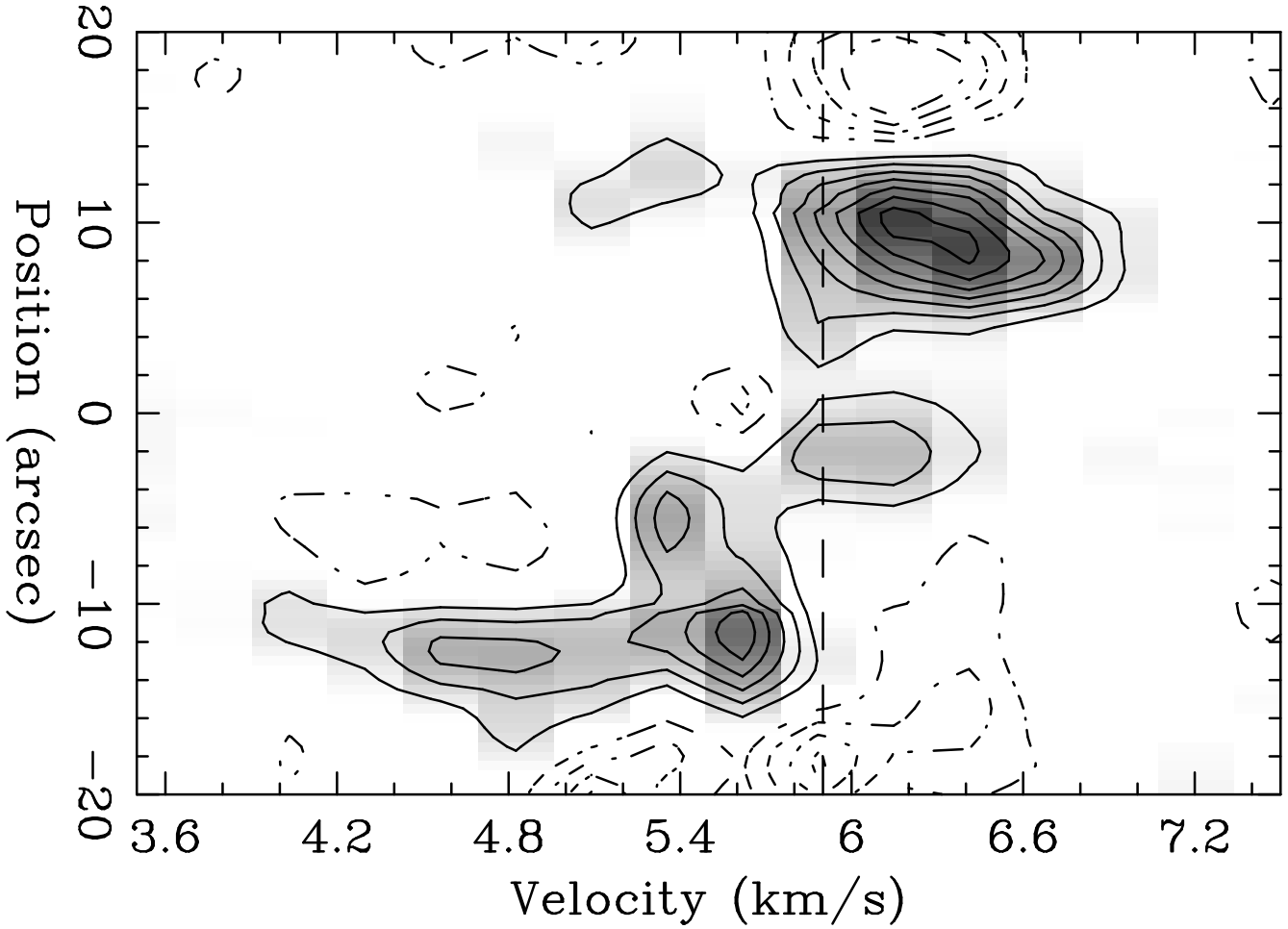


FIG. 2.— Position-Velocity (PV) cut diagram for CO $J = 2 \rightarrow 1$ emission at a position angle of 3° . The contours are $-12, -9, -6, -3, 3, 6, 9, 12, \dots$ times the rms of 0.2 Jy beam^{-1} . The systemic velocity of the brown dwarf, which is estimated by an average of the velocities of red- and blue-shifted components, is indicated by the dashed line. Our value of $5.9 \pm 0.27 \text{ km s}^{-1}$ is consistent with the previously measured value (Whelan et al. 2005) of $7 \pm 8 \text{ km s}^{-1}$ within the error bar. Both blue- and red-shifted components shows a wide range of the velocity in their structure, which appears to be the bow-shock surfaces as observed in young stars (Lee et al. 2000). These surfaces are formed at the head of the jet and accelerate the material in the bow-shock sideways (e.g., Masson & Chernin 1993).

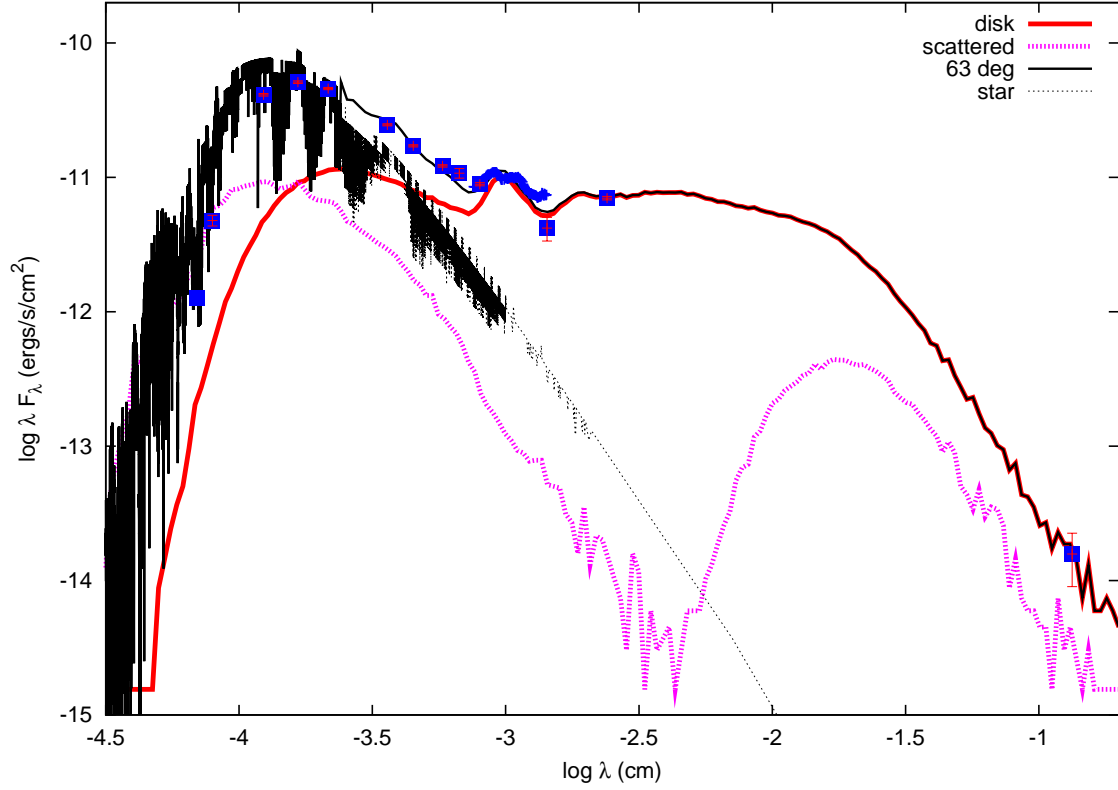


FIG. 3.— Best fit model for ISO-Oph 102. Contributions from the stellar photosphere, the disk and the scattered flux are indicated. Optical and near-infrared data collected from the Vizier archive, infrared fluxes from Natta et al. (2002) and measured based on data from the Spitzer archive (IRAC, MIPS, IRS), millimeter data from our observations.

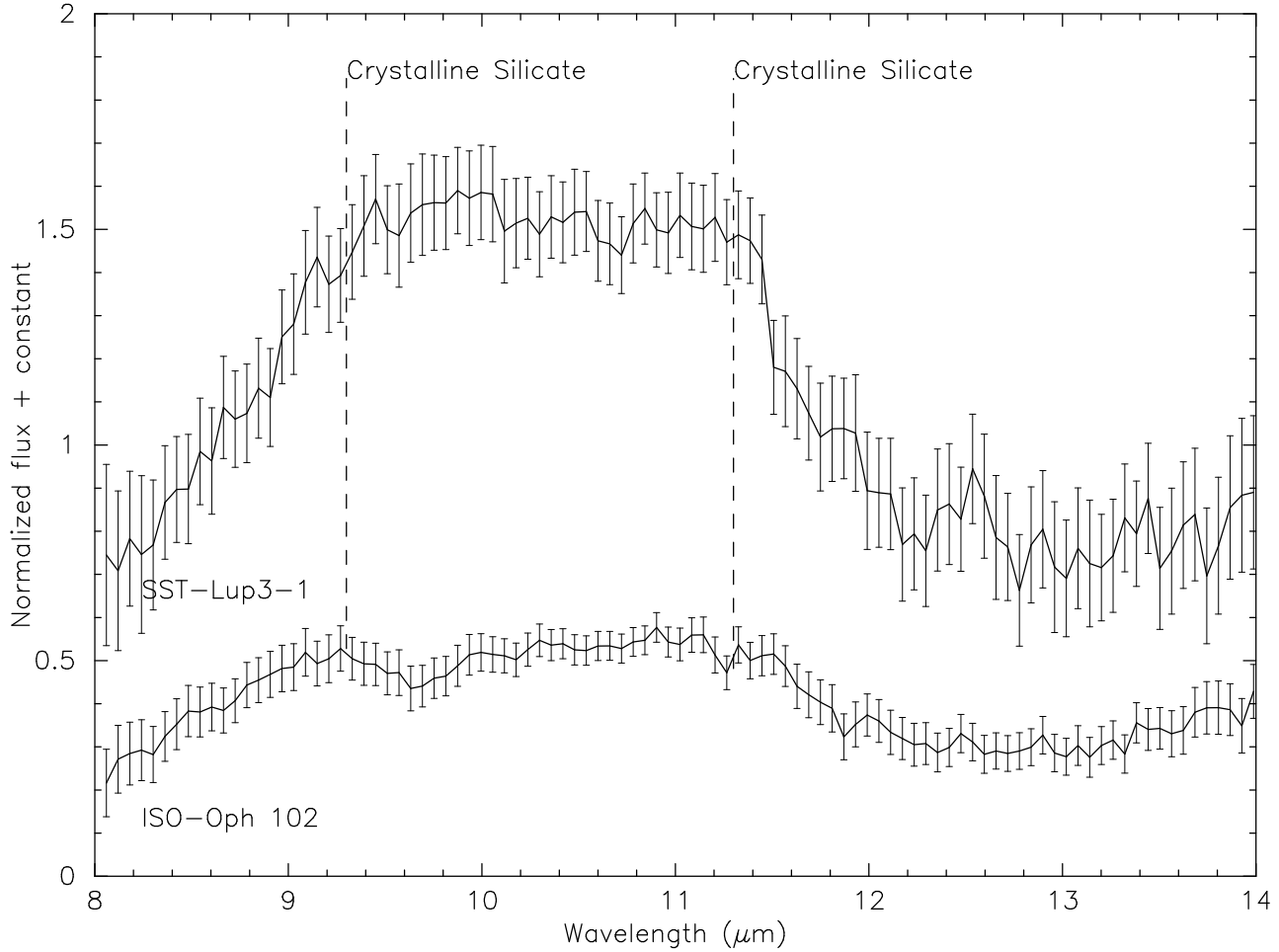


FIG. 4.— Infrared spectral comparison between ISO-Oph 102 and SST-Lup3-1 (Merín et al. 2007) whose spectrum obtained from the Spitzer archival data (PID: 179). Continuum subtraction was done following the literature (van Boekel et al. 2003; Apai et al. 2005). The crystalline silicate features at 9.3 μm (mainly enstatite) and 11.3 μm (forsterite) are indicated.